



# An applicable orthotropic creep model for wood materials and composites

Rhodel Bengtsson<sup>1</sup> · Reza Afshar<sup>1</sup> · E. Kristofer Gamstedt<sup>1</sup> 

Received: 2 February 2022 / Accepted: 13 October 2022 / Published online: 1 November 2022  
© The Author(s) 2022

## Abstract

Despite the engineering importance of creep of composite materials and other fibrous anisotropic load-carrying materials like wood, there is an apparent lack in useful experimental data in 3D. Proposed creep models are generally not commensurate with realistic data from experimental characterization. In the present study, an orthotropic linear viscoelastic model is presented and examined on its performance of predicting the time-dependent nature of wood and composite materials. The constitutive equations are presented using the hereditary approach. A clear description of the finite element implementation of the material model is given. Since constant Poisson's ratios are a common assumption for viscoelastic composites due to lack of data, this study presents the effects of time-dependent Poisson's ratio in the study. The model is calibrated against inevitably asymmetric experimental creep data using an optimization approach. With time-dependent Poisson's ratios, the results show that the model is able to simultaneously capture the time-dependent behaviour in three material axis of orthotropic materials such as European beech wood and a fibre-reinforced composite. However, a relatively poor match was found when the Poisson's ratios were set to be constant. Thus, the frequently employed assumption of constant Poisson's ratios should be made with caution.

---

Reza Afshar and E. Kristofer Gamstedt contributed equally to this work.

---

✉ E. Kristofer Gamstedt  
kristofer.gamstedt@angstrom.uu.se

Rhodel Bengtsson  
rhodel.bengtsson@angstrom.uu.se

Reza Afshar  
reza.afshar@angstrom.uu.se

<sup>1</sup> Division of Applied Mechanics, Department of Materials Science and Engineering, Uppsala University, Box 35, 75103 Uppsala, Sweden

## Introduction

Creep of composites and other fibre-based load-carrying materials, typically result in increasing structural deformations. In engineering, creep of for example composite rotors may lead to deformations that compromise their mechanical function and lead to failure as seen in the paper of Tzeng (2003). In structures based on wood and wood-plastic composites, creep is a design concern that is showcased in the works of Alrubraie et al. (2020), Morlier (1994) and Holzer et al. (1989). In creep of most engineering structures, the stress-state is generally not uniaxial. Composite and wood-based materials are generally anisotropic, and the deformation behaviour is thus different in different directions. It is often sufficient to assume that these materials are orthotropic to capture the main deformations. Another frequent simplifying assumption is the linear viscoelastic behaviour (Afshar et al. 2020), i.e. the strains are linearly dependent on the stress history. Creep testing in several axial directions, including shear, is thus necessary to obtain a creep model which is able to predict deformations in the orthotropic case. Such a full set of experimental data are generally not available, and further assumptions are typically needed to conceive a useful three dimensional (3D) model, which may be used in deformation predictions of complex-shaped structures using finite-element analyses. These assumptions should preferably be made based on the material behaviour and sound engineering arguments. Creep models presented in the literature are either too general with a large number of fitting parameters, or too simple, i.e. one-dimensional only, to predict deformations in several directions. This paper aims to fill this gap by presenting a balanced model apposite to experimental data and the desired predictive capability.

There has been extensive research on the viscoelastic properties of timber structures and composites. Some recent viscoelastic modeling of such materials is presented first, before showing the advantages of the present approach in the context of creep modelling balancing limited materials data and predictability. The approach does not discriminate between composite and wood materials. These may be regarded as examples of orthotropic materials, for which the procedure is intended.

The studies by Vidal-Sallé and Chassagne (2007), Fortino et al. (2009) and Huč and Svensson (2018a) are based on differential approaches by a combination of dashpots and springs in their viscoelastic models for timber. These models take into account a number of phenomena particular to wood materials, such as effects of moisture content and mechanosorption. A challenge when using these models is often to experimentally identify all the parameters needed in the model. In Vidal-Sallé and Chassagne (2007), a full 3D constitutive law is proposed for orthotropic nonlinear viscoelastic behaviour. Their model is based on a rheological generalized Maxwell model with two elements in parallel in addition to a single linear spring. The dashpots of the two Maxwell elements are nonlinear to take into account mechanosorptive nonlinearities. Fortino et al. (2009), contrary to Vidal-Sallé and Chassagne (2007), used a generalized Kelvin model with nonlinear elements to take into account the hygroexpansion effects, viscoelastic creep and mechanosorption.

In the study by Huč and Svensson (2018a), a three-dimensional (3D) rheological model for an orthotropic material is presented. The model is an extension of the two-dimensional (2D) model developed by the same authors (Huč and Svensson 2018b) and is also based on the idea of combining dashpots and springs in different orientations. Using different experimental creep data from the literature and calibrating the model parameters accordingly, the model is able to predict the time-dependent response in three material directions simultaneously.

The anisotropic linear viscoelastic models by Abouhamzeh et al. (2015), Zocher and Groves (1997) and White and Kim (1998) used the hereditary approach to account for the thermo-viscoelastic behaviour of composite material in order to estimate the residual stresses during cool-down. The analysis has been shown to be useful in prediction of residual stresses during production of composite components and also in varying thermal environments. Only the thermo-viscoelastic behaviour of the polymer constituent is characterized, from which the composite properties are estimated. In Abouhamzeh et al. (2015), the properties of the orthotropic material are calculated in the Laplace domain and used as input to the subroutine provided to the material model in ANSYS.

Nonlinear viscoelastic models require creep data at many stress levels. Available data are generally limited to only a few stress levels. A linear viscoelastic model is therefore often the immediate choice. In primary and secondary creep, covering the largest portion of creep life, it can be fair to assume linearity. Most structures are designed in such a way that stress levels are much smaller than strength values, in a regime where the material is likely to show a linear behaviour.

In linear viscoelastic models, the elastic moduli are considered to be dependent on time only. The aforementioned models in Fortino et al. (2009), Vidal-Sallé and Chassagne (2007), Huč and Svensson (2018a) and Huč and Svensson (2018b) have been able to display the time-dependent Poisson's effect. In Zocher and Groves (1997) and White and Kim (1998), constant Poisson's ratios are assumed for their models. This is not often experimentally the case as seen in Pandini and Pegoretti (2008). Another effect that is largely unaddressed is that experiments typically show asymmetric relaxation and compliance matrices which is shown by works of both Ozyhar et al. (2013) and Endo and de Carvalho Pereira (2017). Additionally, in the works of Ando et al. (2013), they highlight the asymmetric behaviour of the creep behaviour of Japanese cypress, but were not able to explain the cause of this behaviour. Obara (2018) tried to verify the commonly assumed elastic orthotropic model of wood by going through the elastic constants available in the literature, and concluded that many of the works found did not satisfy the symmetry conditions. One plausible theory to explain the asymmetry stem from the inaccuracy of the measuring equipment which is discussed by Bodig and Jayne (1982) and Gonçalves et al. (2011). High precision measurements are difficult, especially when measuring strains perpendicular to the loading direction, which is often several of magnitudes smaller than the strains parallel to the loading. Another source of asymmetry might be from the specimen itself due to imperfection and orientation of the material direction inside. Finally, as discussed in Garab et al. (2010), since wood is a natural material, its irregular

cell-structure in the micro-scale might introduce some nonlinear behaviour that might be perceived as asymmetry in the macro-scale.

In this paper, the hereditary approach is used to represent the viscoelastic behaviour of orthotropic materials, of which its derivation and finite element derivation is well explained in the following section. The parameters of the two-term Prony series model are calibrated with experimental creep data, as a balance between under and over-fitting. Two assumptions concerning the Poisson’s ratios were considered: time dependent and constant. Furthermore, a straightforward approach how to deal with the inevitable asymmetric behaviour of experimental data is presented. The overall scheme is schematically illustrated in Fig. 1.

### Theoretical background

In this section, the theoretical background of the orthotropic linear viscoelastic model is presented by means of the hereditary approach, which in turn serves as input in the numerical implementation.

In linear viscoelasticity, the stress can be expressed by the convolution integral, Starting from an unloaded and completely relaxed state at  $t = 0^-$ ,

$$\sigma_i(t) = C_{ij}(t)\epsilon_j(0) + \int_0^t C_{ij}(t-s)\dot{\epsilon}_j(s)ds. \tag{1}$$

where  $\sigma_i$  and  $\epsilon_i$  are stress and strains in index form using the Voigt notation, and  $C_{ij}$  are the components of the time-dependent (relaxation) stiffness matrix. Furthermore,  $C_{ij}$  is assumed to be described by a Prony series

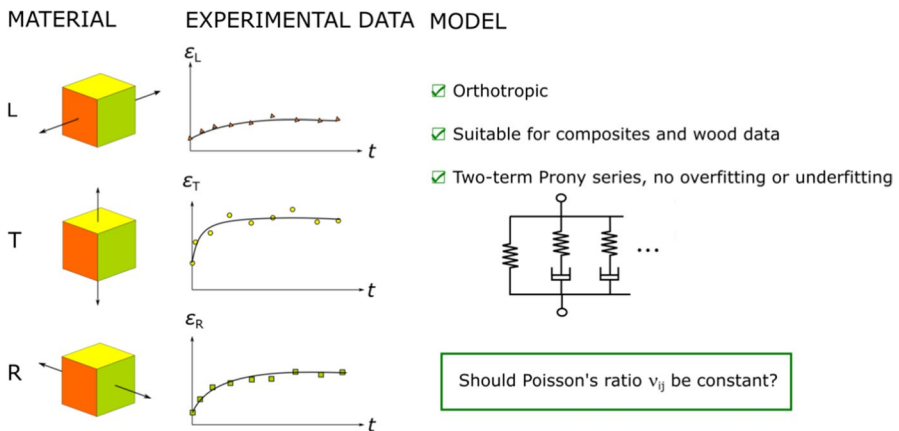


**Fig. 1** Schematic illustration of the present investigation, where existing experimental data for orthotropic materials is captured by well-balanced rheological model

$$C_{ij}(t) = C_{ij}^{\infty} + \sum_{k=1}^M C_{ij}^{(k)} e^{-\frac{t}{\tau_{ij}^{(k)}}}, \quad (2)$$

where  $C_{ij}^{\infty}$ ,  $C_{ij}^{(k)}$  and  $\tau_{ij}^{(k)}$  are the model parameters that will be determined in the section “[Determination of the model parameters](#)”, and  $M$  is the number of terms used in the Prony series and  $k$  is the index of summation that has a lower bound of unity and an upper bound of  $M$ . Equation (2) is analogous to the 1D Prony series model which is well presented in the works of Tschoegl (2012) and Ottosen and Ristinmaa (2005). The instantaneous static behaviour is described using Eq. (2) in Eq. (1) at  $t = 0$ ,

$$\sigma_i(0) = C_{ij}(0)\varepsilon_j(0) = \left[ C_{ij}^{\infty} + \sum_k C_{ij}^{(k)} \right] \varepsilon_j(0). \quad (3)$$

The stress at an arbitrary time  $t$  can be obtained using a recurrence relation by combining Eqs. (1) and (2), resulting in the following expression:

$$\sigma_i(t) = \left[ C_{ij}^{\infty} + \sum_k C_{ij}^{(k)} e^{-\frac{t}{\tau_{ij}^{(k)}}} \right] \varepsilon_j(0) + \int_0^t \left[ C_{ij}^{\infty} + \sum_k C_{ij}^{(k)} e^{-\frac{t-s}{\tau_{ij}^{(k)}}} \right] \dot{\varepsilon}_j(s) ds, \quad (4)$$

which in return can be separated in an elastic and several viscous parts, namely

$$\sigma_i(t) = \sigma_{i,\text{elastic}}(t) + \sum_{k=1}^M \sigma_{i,\text{viscous}}^{(k)}(t) \quad (5)$$

where,

$$\sigma_{i,\text{elastic}} = C_{ij}^{\infty} \left( \varepsilon_j(0) + \int_0^t \dot{\varepsilon}_j(s) ds \right) = C_{ij}^{\infty} \varepsilon_j(t) \quad (6)$$

and,

$$\sigma_{i,\text{viscous}}^{(k)} = C_{ij}^{(k)} \left( e^{-\frac{t}{\tau_{ij}^{(k)}}} \varepsilon_j(0) + \int_0^t e^{-\frac{t-s}{\tau_{ij}^{(k)}}} \dot{\varepsilon}_j(s) ds \right) \quad (7)$$

In a stepwise integration, it is useful to evaluate the integral in Eq. (7) by separating it into two domains  $s = [0, t - \Delta t]$  and  $s = [t - \Delta t, t]$ , resulting in

$$\sigma_{i,\text{viscous}}^{(k)} = C_{ij}^{(k)} \left( e^{\frac{-t}{\tau_{ij}^{(k)}}} \epsilon_j(0) + \int_0^{t-\Delta t} e^{\frac{-(t-s)}{\tau_{ij}^{(k)}}} \dot{\epsilon}_j(s) ds + \int_{t-\Delta t}^t e^{\frac{-(t-s)}{\tau_{ij}^{(k)}}} \dot{\epsilon}_j(s) ds \right) \tag{8}$$

From Eq. (7), the viscous stresses are evaluated at time  $t - \Delta t$ ,

$$\begin{aligned} \sigma_{i,\text{viscous}}^{(k)}(t - \Delta t) &= C_{ij}^{(k)} \left( e^{\frac{-(t-\Delta t)}{\tau_{ij}^{(k)}}} \epsilon_j(0) + \int_0^{t-\Delta t} e^{\frac{-(t-\Delta t-s)}{\tau_{ij}^{(k)}}} \dot{\epsilon}_j(s) ds \right) \\ &= C_{ij}^{(k)} e^{\frac{-\Delta t}{\tau_{ij}^{(k)}}} \left( e^{\frac{-t}{\tau_{ij}^{(k)}}} \epsilon_j(0) + \int_0^{t-\Delta t} e^{\frac{-(t-s)}{\tau_{ij}^{(k)}}} \dot{\epsilon}_j(s) ds \right) \end{aligned} \tag{9}$$

Since the terms in Eq. (9) may be found in Eq. (8), the current viscous stresses are described by the viscous stresses at  $t = t - \Delta t$  such as

$$\sigma_{i,\text{viscous}}^{(k)} = e^{\frac{-\Delta t}{\tau_{ij}^{(k)}}} \sigma_{i,\text{viscous}}(t - \Delta t) + C_{ij}^{(k)} \int_{t-\Delta t}^t e^{\frac{-(t-s)}{\tau_{ij}^{(k)}}} \dot{\epsilon}_j(s) ds \tag{10}$$

### Finite element implementation

To implement a material model in a commercial finite element software such as ANSYS mechanical APDL, it is convenient to calculate the stress based on a strain increment and the information of the previous time steps. This is done by using the relaxation form to derive the viscoelastic constitutive equations. For small time steps  $\Delta t$ , the strain rate  $\dot{\epsilon}_j$  may be considered constant,

$$\dot{\epsilon}_j = \frac{\Delta \epsilon_j}{\Delta t}, \tag{11}$$

and thus Eq. (10) transforms into

$$\sigma_{i,\text{viscous}}^{(k)} = e^{\frac{-\Delta t}{\tau_{ij}^{(k)}}} \sigma_{i,\text{viscous}}(t - \Delta t) + \frac{1 - e^{\frac{-\Delta t}{\tau_{ij}^{(k)}}}}{\Delta t / \tau_{ij}^{(k)}} C_{ij}^{(k)} \Delta \epsilon_j \tag{12}$$

From Eq. (12), it is now possible to obtain the viscous stresses from each time step  $\Delta t$ . It is noted that the viscous stresses at time  $t$  are equal to a fraction of the viscous

stress from the previous time step plus a stress increment due to the strain increment  $\Delta\varepsilon_j$ . Finally, the total stress is the sum of the elastic and viscous contributions,

$$\begin{aligned} \sigma_i(t) = & C_{ij}^\infty \varepsilon_j(t) + \sum_{k=1}^M e^{\frac{-\Delta t}{\tau_{ij}^{(k)}}} \sigma_{i,\text{viscous}}(t - \Delta t) \\ & + \sum_{k=1}^M \frac{1 - e^{\frac{-\Delta t}{\tau_{ij}^{(k)}}}}{\Delta t / \tau_{ij}^{(k)}} C_{ij}^{(k)} \Delta\varepsilon_j \end{aligned} \quad (13)$$

In addition to the stress update, it is necessary to provide the consistent tangent stiffness, also known as the material Jacobian, to the finite element (FE) software. The consistent tangent stiffness is necessary to derive the constitutive component of the internal virtual work, where the latter is discretized to formulate the FE equations which is later solved via Newton–Raphson iterations to find the corresponding displacements that yield equilibrium. Deriving Eq. (13) with respect to the strain  $\varepsilon_j$ , the Jacobian is obtained,

$$C_{ij}^{\text{tan}} = \frac{\partial \sigma_i(t)}{\partial \varepsilon_j(t)} = C_{ij}^\infty + \sum_{k=1}^M \frac{1 - e^{\frac{-\Delta t}{\tau_{ij}^{(k)}}}}{\Delta t / \tau_{ij}^{(k)}} C_{ij}^{(k)} \quad (14)$$

From Eq. (2), it should be noted that this approach will have  $9 + 18M$  parameters that need to be defined in order to fully describe the viscoelasticity of a general 3D orthotropic material. Choosing an adequate number of parameters is often a challenging task. On the one hand, overfitting by too many empirical parameters does not add any significant predictive precision given the generally large scatter in measured data. On the other hand, underfitting with too few parameters will not capture the main traits of the time-dependent load–deformation behaviour.

### Determination of the model parameters

Given that creep experiments in all directions have been performed, the parameters of the model may readily be identified. The (relaxation) stiffness matrix  $\mathbf{C}$  in Eq. (2) is assumed to be the inverse of the (creep) compliance matrix  $\mathbf{D}$  where

$$\mathbf{D} = \begin{bmatrix} \frac{1}{E_L} & \frac{-\nu_{LR}}{E_R} & \frac{-\nu_{LT}}{E_T} & 0 & 0 & 0 \\ \frac{-\nu_{RL}}{E_L} & \frac{1}{E_R} & \frac{-\nu_{RT}}{E_T} & 0 & 0 & 0 \\ \frac{-\nu_{TL}}{E_L} & \frac{-\nu_{TR}}{E_R} & \frac{1}{E_T} & 0 & 0 & 0 \\ 0 & 0 & 0 & \frac{1}{G_{LR}} & 0 & 0 \\ 0 & 0 & 0 & 0 & \frac{1}{G_{LT}} & 0 \\ 0 & 0 & 0 & 0 & 0 & \frac{1}{G_{RT}} \end{bmatrix} \tag{15}$$

in the orthotropic case (L: Longitudinal, R: Radial and T: Tangential).

It should be emphasized that each element in the compliance matrix, as well as its components, is time dependent. The time-dependent Poisson’s ratios are defined as discrete points in time, such

$$\nu_{ij}(t_n) = -\frac{\varepsilon_j(t_n)}{\varepsilon_i(t_n)}. \tag{16}$$

which are determined by the strain in the lateral direction of the creep test,  $\varepsilon_j$ , and the strain in the loading direction of the same creep test,  $\varepsilon_i$ . Likewise, the time-dependent Young’s moduli are also defined as discrete points in time

$$E_i(t_n) = \frac{\sigma_i}{\varepsilon_i(t_n)} \tag{17}$$

which are determined by the constant creep stress  $\sigma_i$  and the resulting strain  $\varepsilon_i$ . Determining the shear moduli  $G_{ij}$  is analogous to Eq. (17).

It is important to keep the compliance matrix as a symmetric matrix in order to invert it and obtain a symmetric stiffness matrix, which is a requirement when implementing it in a FE software as a linear problem. Experimentally, the compliance matrix is never fully symmetric (e.g. see Ozyhar et al. 2013; Rogers and Pipkin 1963). The matrix can be made symmetric in different ways. The simplest way being the averaging of the off-diagonal elements of the compliance matrix. However, in this study the symmetry is enforced by mixing the off-diagonal terms into one term by using a weighting variable  $x$ , see Eq. (18). Consider two separate uniaxial tensile creep tests (in 2D) in which constant stresses,  $\sigma_L$  and  $\sigma_R$ , are applied in each test, respectively. The constant stress  $\sigma_L$  is applied in the longitudinal direction, resulting in a creep strain  $\varepsilon_L^L(t)$  in the loading direction, and creep strain  $\varepsilon_R^L(t)$  in the radial direction due to the Poisson effect. Similarly, the constant stress  $\sigma_R$  is applied in the radial direction, resulting in a creep strain  $\varepsilon_R^R(t)$  in the loading direction, and creep strain  $\varepsilon_L^R(t)$  in the longitudinal direction due to the Poisson effect. Inserting Eqs. (16) and (17), allows us to calculate the off-diagonal elements  $D_{21}$  and  $D_{12}$  in Eq. (15) as discrete points. It is expected that  $D_{12}$  and  $D_{21}$  are not equal to each other from the experiments, and thus a weighted operation has to be made to make the compliance matrix symmetric. For instance, one can define a new diagonal element  $D_{12}^{\text{sym}}$  such that



$$D_{12}^{\text{sym}} = xD_{12} + (1 - x)D_{12}, \quad (18)$$

where  $x$  is decided by minimizing the absolute error in terms of Euclidean norms,

$$\epsilon = \| \epsilon_R^L - D_{12}^{\text{sym}}(x)\sigma_L \| + \| \epsilon_L^R - D_{12}^{\text{sym}}(x)\sigma_R \|. \quad (19)$$

$D_{12}^{\text{sym}}$  is meant to replace the off-diagonal terms  $D_{12}$  and  $D_{21}$  in the compliance matrix, thus the same operations can be made on  $D_{13}$  and  $D_{31}$  (longitudinal and tangential) and  $D_{23}$  and  $D_{32}$  (radial and tangential), respectively. When  $D_{ij}$  are fully defined,  $C_{ij}$  are defined by means of inversion. Note that the elements of  $C_{ij}$  are still discrete points in time and need to be curve-fitted to follow Eq. (2) using any curve-fitting algorithm/software of choice.

## Numerical implementation

The proposed model was implemented in the ANSYS subroutine USERMAT to describe the viscoelastic behaviour of common orthotropic materials. The model parameters  $C_{ij}^{\infty}$ ,  $C_{ij}^k$  and  $\tau_{ij}$  are determined by calibrating against measured creep data from various experimental studies using MATLAB function `lsqcurvefit`. The compliance matrix was rendered symmetric by minimizing the absolute errors as described in the "[Determination of the model parameters](#)" section with Eqs. (18) and (19), using the same MATLAB fitting function. For lack of shear creep data in the literature, the shear components are not included here. Each component of the stiffness matrix was described with one constant value and two exponential terms in the Prony series, meaning in Eq. (2),  $M = 2$ . The variability of data does not motivate more exponential terms. With fewer terms, the main characteristics of the creep curves cannot be captured which was concluded from a pre-study.

For the time-integration scheme, the Newmark-Beta method with default parameters was chosen in Ansys. The time-stepping during the solution was automatic, but the maximum time step was determined from a pre-study for each loading direction. In the pre-study, the maximum time step was halved until the relative difference between the final creep strains (in all directions) at  $t = \text{end}$  was 0.1%.

As mentioned previously, many authors such as Abouhamzeh et al. (2015), White and Kim (1998) and Melo and Radford (2003) assume that the Poisson's ratio is constant, although it has not been shown that this is a fair assumption in general. Therefore, we consider the two cases, where (i) the Poisson's ratio is time dependent, and (ii) the Poisson's ratio is constant and does not vary with time, i.e.  $\nu_{ij}(t)$  in Eq. (16) is replaced with

$$\nu_{ij} = -\frac{\epsilon_j(t=0)}{\epsilon_i(t=0)}. \quad (20)$$

The comparison of the two cases in light of experimental data can show if the simplifying assumption of constant Poisson's ratios significantly impairs the accuracy

of the model. Such assessment applied to orthotropic creep data in the literature has so far not been found to the knowledge of the authors.

Two examples of a cube in solid wood and one of fibre-reinforced composite material are demonstrated. The cubes with unit edge lengths are modelled in Ansys Mechanical APDL. The cube edge length was arbitrarily taken to be 1 mm, although the length has no effect on the results in these simulations since there is no length-scale effect in the model. The cube itself is meshed by a single trilinear hexahedral element, which is separately loaded in the three perpendicular material axes. The performance of the numerical model is measured by the coefficient of determination,  $R^2$ , as recommended by for example Hines and Montgomery (1980). However, this statistic measure should be used with caution as it is possible to get a “perfect fit” by forcing the model to go through all the data points by increasing the amount of model parameters without considering what happens between the data points. Thus, it is also important to plot the model and data points for qualitative comparisons.

### European beech wood

Ozyhar et al. (2013) performed a tensile creep test of European beech wood to highlight the unequal time dependency of the Young’s moduli and the Poisson’s ratios obtained. The samples were of thick dogbone shape and the creep tests were carried out in a constant climate test room under controlled environmental conditions. The creep test was realized with a universal testing machine with a load cell of 10 kN, with three samples per loading direction. To avoid mechanosorptive creep, the samples were pre-conditioned and reached their moisture equilibrium in the same climate condition as before testing. The creep load was adjusted depending on which material direction as parallel to the loading direction. For radial and tangential direction, the load level was set to 75% of the yield stress defined in the direction. When loading in the longitudinal direction, the load level was of 25% of the ultimate strength in the longitudinal direction. The load levels in the experiment were well within the linear viscoelastic assumption according to Ozyhar et al. (2013). The creep strains are captured via digital image correlation. The resulting creep curves are shown for each loading direction in Fig. 2 for longitudinal (L), Fig. 3 for tangential (T) and Fig. 4 for radial (R).

It is readily possible to take into account either fully time-dependent or constant (time invariant) Poisson’s ratios in the model. Additionally, one can choose which specific Poisson’s ratios are to be constant or allowed to be time dependent. This selection can be done by identifying which Poisson’s ratio changes the least in comparison with the others. In the experiment of Ozyhar et al. (2013), it was identified that  $\nu_{RL}$ ,  $\nu_{TL}$  and  $\nu_{RT}$  did not change as fast as the remaining three Poisson’s ratios, perhaps due to the stiffening effect of radial rays prevalent in hardwoods. Thus, the assumption of having these specific ratios to be time-independent was implemented into the model as well as a third case.

The first curves in Figs. 2, 3 and 4 are the un-constrained model of which all the Poisson’s ratios are fully time dependent. Using the creep strains from the experiments of Ozyhar et al. (2013), Eq. (16) was used to get the time-dependent

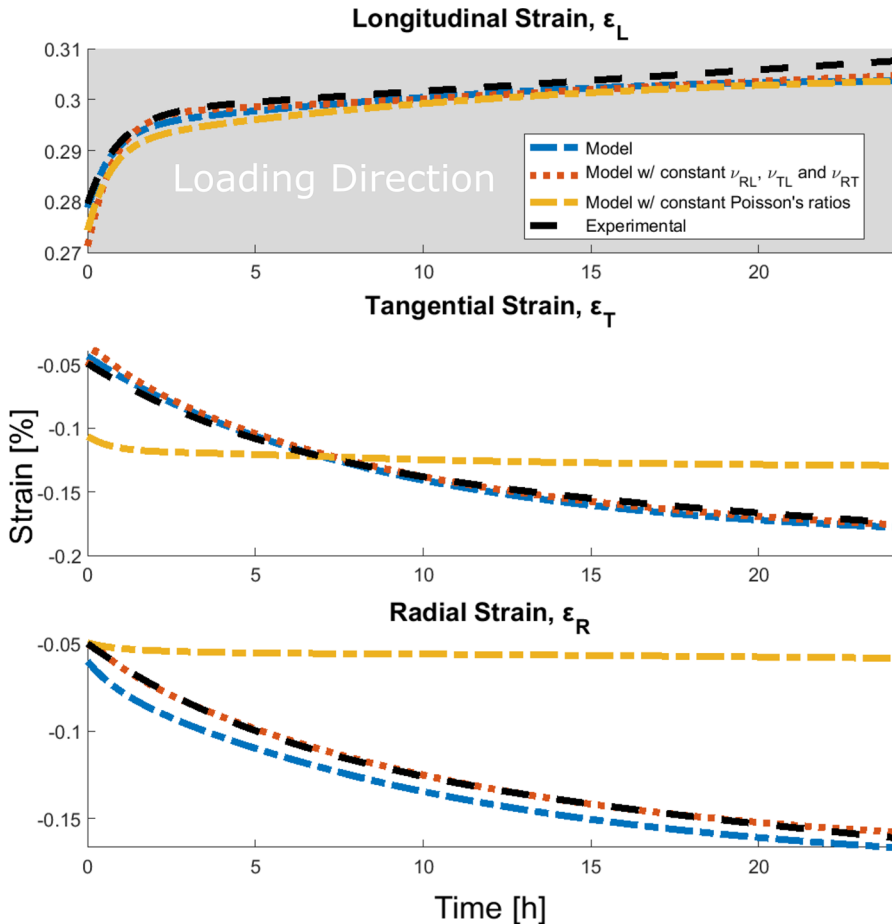


**Fig. 2** Comparison of creep curves between experimental measurement and viscoelastic models with time-dependent and (some) constant Poisson's ratios. Creep curves are presented in the longitudinal,  $\epsilon_L$ , tangential direction,  $\epsilon_T$ , and radial direction,  $\epsilon_R$ , during tensile loading in the longitudinal direction (L). The experimental data for beech wood are from Ozyhar et al. (2013)

Poisson's ratios. For the time-invariant Poisson's ratios, we took the initial elastic strains from the experimental creep data at  $t = 0$  and thus use Eq. (20) to compute that assumed constant ratio. This procedure was done for all of the Poisson's ratios for the fully constant assumption and done for  $\nu_{RL}$ ,  $\nu_{TL}$  and  $\nu_{RT}$  for the semi-constant assumption. When we have both the Poisson's ratios from either Eqs. (16) or (20) and the Young's moduli from Eq. (17), these parameters were inserted into the creep compliance matrix in Eq. (15). Since the compliance matrix is not symmetric in general, as enforced symmetry by replacing the off-diagonals in the matrix by a mixture of the terms through Eqs. (18) and (19). The model parameters for each model are given in the tables in the supplemental material.

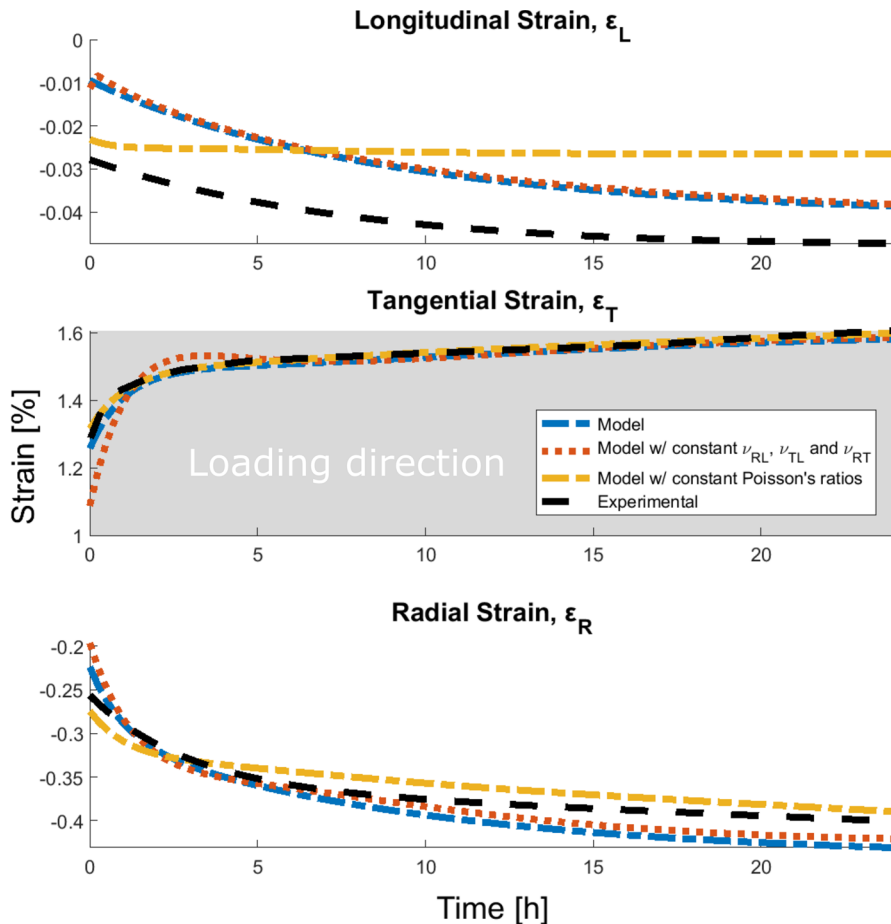


**Fig. 3** Comparison of creep curves between experimental measurement and viscoelastic models with time-dependent and (some) constant Poisson's ratios. Creep curves are presented in the longitudinal,  $\epsilon_L$ , tangential direction,  $\epsilon_T$ , and radial direction,  $\epsilon_R$ , during tensile loading in the tangential direction (T). The experimental data for beech wood are from Ozyhar et al. (2013)

### Fibre-reinforced composite material

Although creep in structures from orthotropic materials is more prominent in wood, it also is of relevance for fibre-reinforced polymer composites (e.g., Tzeng 2003). To demonstrate the generality of the present approach beyond wood materials, an application for a fibre-reinforced composite material is shown. Endo and de Carvalho Pereira (2017) performed an approximately 3.5 weeks long tensile creep test of a glass-fibre-reinforced thermoplastic composite at a temperature of 23.5 °C. The samples were taken from injection-moulded plates of short-fibre-reinforced polybutylene terephthalate in a region with a uniform in-plane fibre

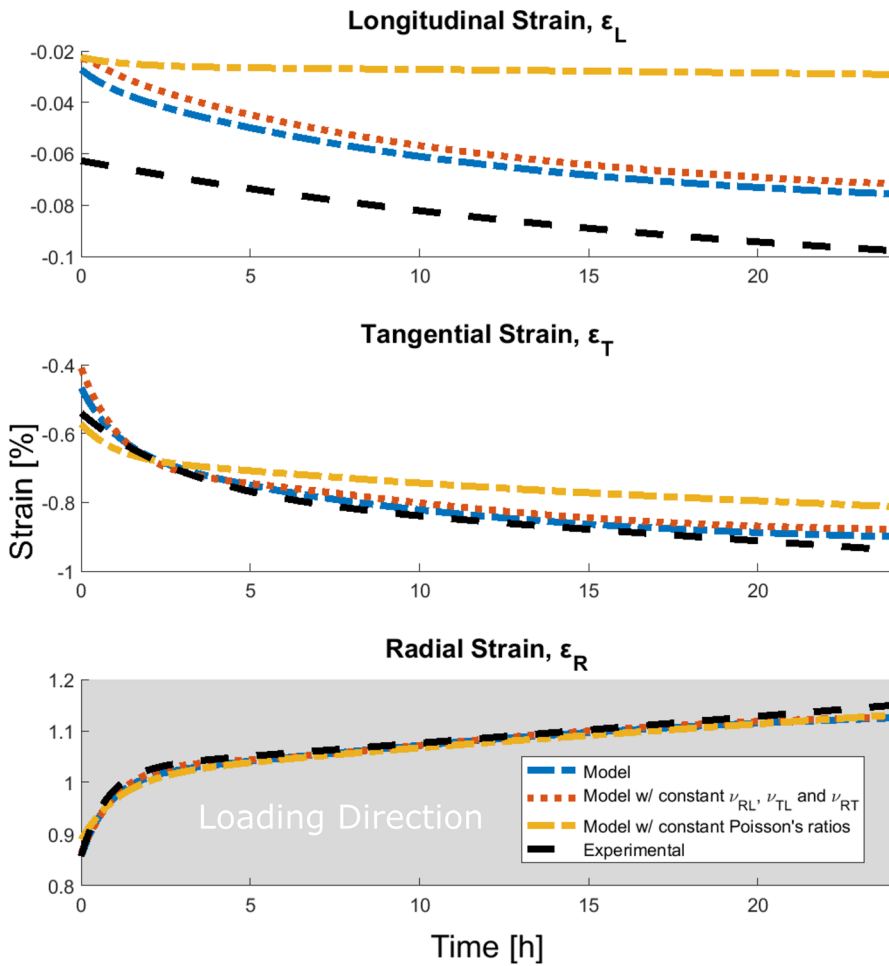


**Fig. 4** Comparison of creep curves between experimental measurement and viscoelastic models with time-dependent and (some) constant Poisson's ratios. Creep curves are presented in the longitudinal,  $\epsilon_L$ , tangential direction,  $\epsilon_T$ , and radial direction,  $\epsilon_R$ , during tensile loading in the radial direction (R). The experimental data for beech wood are from Ozyhar et al. (2013)

orientation distribution making the material essentially orthotropic. Two loading directions were used, parallel and perpendicular to the main material axis, denoted as the longitudinal (L) and transverse (T) direction, respectively. A tensile stress of 12 MPa was applied to both cases. The resulting creep curves are shown in equal dashed lines for each loading direction, i.e. Fig. 5 in the longitudinal direction and Fig. 6 in the transverse direction, showing the resulting creep strains in the longitudinal direction,  $\epsilon_L$  and in the transverse direction,  $\epsilon_T$ . The models in Figs. 5 and 6 are made in the same way as described in the previous

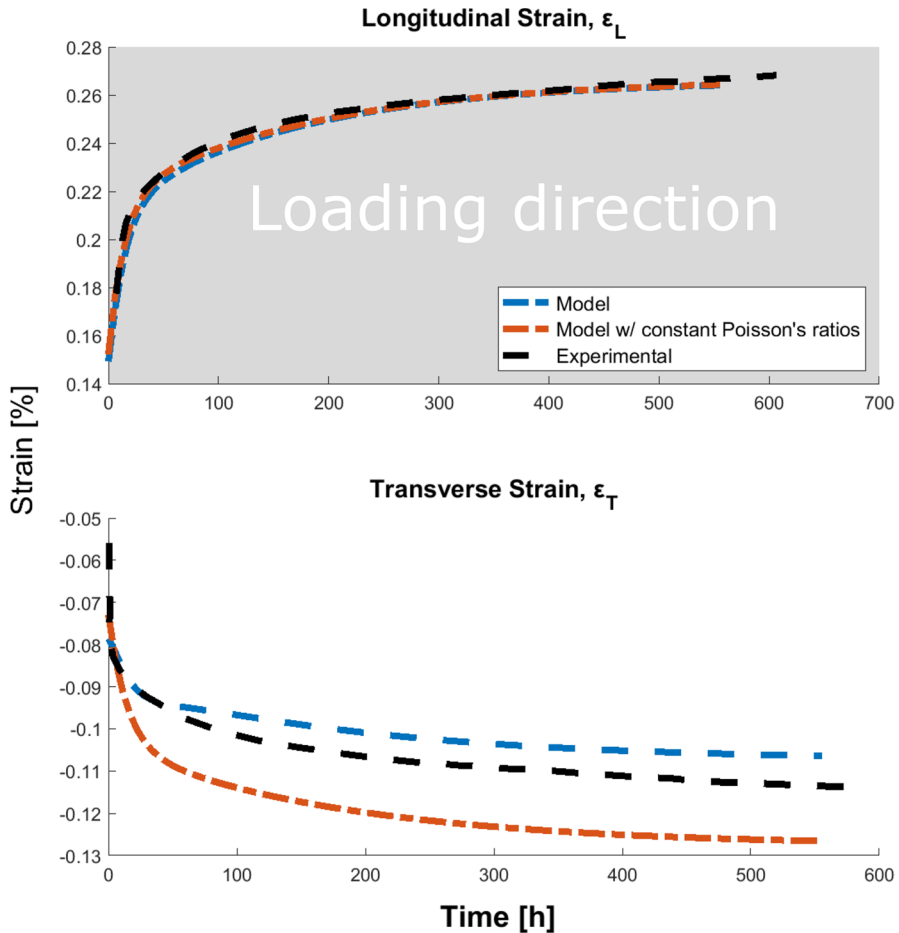


**Fig. 5** Comparison of creep curves between experimental measurement and viscoelastic models with time-dependent and constant Poisson's ratios. Creep curves are presented in the longitudinal,  $\epsilon_L$ , and transverse direction,  $\epsilon_T$ , during tensile loading longitudinal direction (L). The experimental data for glass-fibre composite material are from Endo and de Carvalho Pereira (2017)

section. The model parameters for each model are given in the tables in the supplemental material.

## Discussion

For both the composite and wood materials, there is a distinct difference in the ability of the confined models to predict creep curves along all material axes depending on whether the Poisson's ratio are restrained to be constant or allowed to be time dependent in terms of a Prony series. However, these trends are different in the two types of material, i.e. the wood material (Figs. 2, 3, 4) and the fibre-reinforced

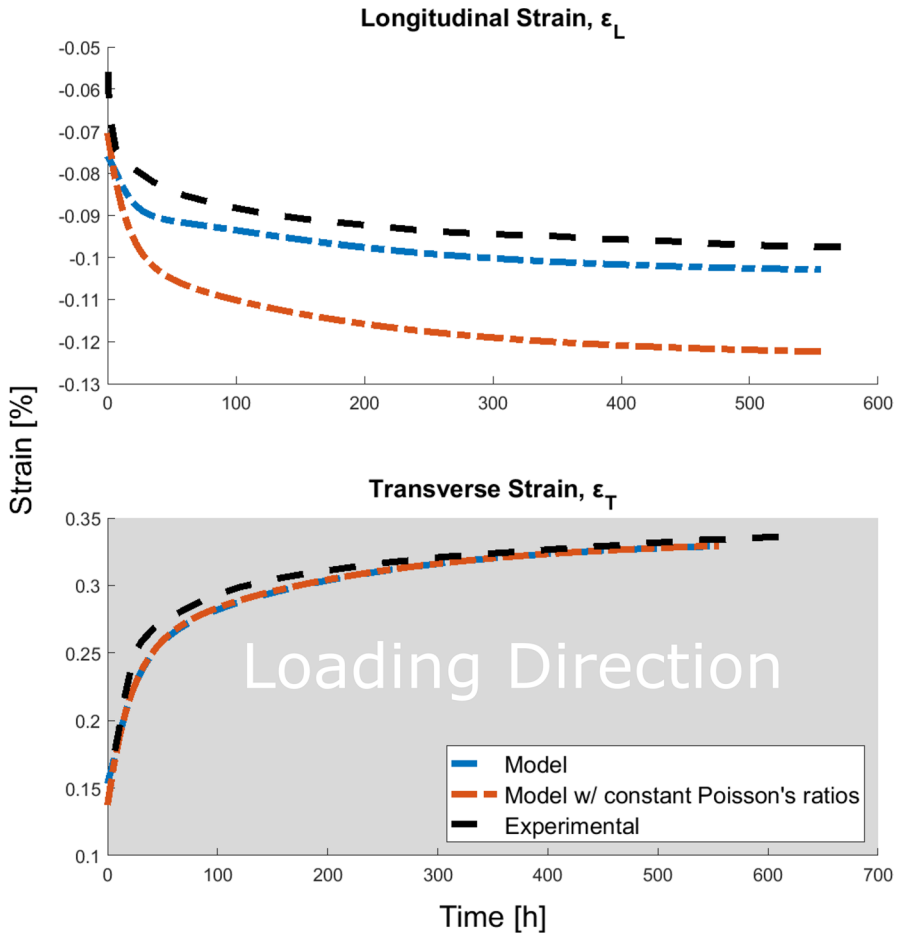


**Fig. 6** Comparison of creep curves between experimental measurement and viscoelastic models with time-dependent and constant Poisson's ratios. Creep curves are presented in the longitudinal,  $\epsilon_L$ , and transverse direction,  $\epsilon_T$ , during tensile loading transverse to the fibre direction (T). The experimental data for a glass-fibre composite material are from Endo and de Carvalho Pereira (2017)

composite (Figs. 5, 6). In the glass-fibre composite material, the assumed constant Poisson's ratios resulted in larger transverse creep in longitudinal loading direction, as shown in Fig. 5. In contrast, the wood sample showed smaller transverse creep when all Poisson's constants were assumed to be constant, as can be seen in Fig. 2. This difference between composite and wood behaviour is most likely a result of the difference in their microstructure, where the composite is composed of fibres and matrix, whereas wood is essentially a cellular material. Nevertheless, it is clear that allowing time-dependent Poisson's ratios, the model could fit very well with the experimental data. The difference or similitude between the results from the model and the experimental data seen in the graphs is also quantified by the coefficient of determination  $R^2$  in Table 1 for the European beech wood material, and in

**Table 1** Coefficient of determination values,  $R^2$ , as a measure to compare the fit to experimental data for beech wood from Ozyhar et al. (2013) for strains  $\epsilon_j^i$ , where  $i$  is the loading direction and  $j$  is direction of measured strain

Strains	Coefficient of determination, $R^2$		
	Model	Model with $\nu_{RL}$ , $\nu_{TL}$ and $\nu_{RT}$ constant	Model with all Poisson's ratios constant
$\epsilon_L^L$	0.9329	0.8442	0.8146
$\epsilon_T^L$	0.9895	0.9980	0.2646
$\epsilon_R^L$	0.9209	0.9984	- 3.3246
$\epsilon_L^T$	- 2.2558	- 2.5471	- 4.6832
$\epsilon_T^T$	0.9411	0.2974	0.9855
$\epsilon_R^T$	0.7374	0.8257	0.8352
$\epsilon_L^R$	- 3.2918	- 5.1936	- 23.8453
$\epsilon_T^R$	0.9537	0.8547	0.3651
$\epsilon_R^R$	0.9640	0.9724	0.9450

Table 2 for the fibre-reinforced composite material. Despite a limited number of fitting parameters, the model with unfixed time-dependent Poisson's ratios shows good match with experimental creep data with high values of  $R^2$ . When the  $R^2$  values are negative, the model does not even follow the trend and leads to a worse fit than just taking the constant average value.

Although fixing the Poisson's ratios in the 2D case for the composite material turned out to be an imprudent choice, fixing some of the Poisson's ratios for the 3D case did not impair the model predictions. Some of the ratios turned out to be essentially time-invariant, viz.  $\nu_{RL}$ ,  $\nu_{TL}$  and  $\nu_{RT}$ , and by setting only these to constants an almost equally good fit was obtained for most directions, as shown in Figs. 2, 3 and 4 and compiled in Table 1. For orthotropic materials in general, it can thus be acceptable to assume constant Poisson's ratios in certain directions. Which Poisson's ratios can be assumed to be constant and which cannot must be confirmed by experimental results. A constant Poisson's ratio means that the strain in the loading direction creeps proportionally to the measured resulting strain in the lateral direction. The underlying reasons for this proportionality, or lack thereof, must be a result of the creep mechanics on the microstructural level. These mechanisms are different for composites [see e.g. Eitelberger et al. (2012) and Wen et al. (1997)], due to the microstructural differences of these materials.

**Table 2** Coefficient of determination values,  $R^2$ , as a measure to compare the fit to experimental data for a glass-fibre composite material from Endo and de Carvalho Pereira (2017) for strains  $\epsilon_j^i$ , where  $i$  is the loading direction and  $j$  is the direction of measured strain

Strains	Coefficient of determination, $R^2$	
	Model	Model with constant Poisson's ratios
$\epsilon_L^L$	0.9746	0.9908
$\epsilon_T^L$	0.7926	0.4221
$\epsilon_L^T$	0.5957	- 2.1578
$\epsilon_T^T$	0.9581	0.9600



In general, the model appears to have some relative difficulties in capturing the Poisson's effect in Figs. 2, 3 and 4 and quantified by  $R^2$  values in Table 1. This is mainly due to the asymmetry of the experimental data and how the off-diagonal components of the compliance matrix were determined. In practice, the experimental behaviour is not fully orthotropic, although an orthotropic model is prescribed to represent the experiments. A result of the minimisation in Eqs. (18) and (19) is that the Poisson's effect in the tangential and radial directions are favoured over the one in the longitudinal direction. Incidentally, this is beneficial from a practical point of view, as the creep in the longitudinal direction in general is often negligible compared to the perpendicular directions. However, if the fitting is unfavourably skewed, it is possible to weight the minimisation problem towards capturing the longitudinal direction if the user so chooses.

It has been shown that it is quite sufficient to use only two exponential terms in the Prony series for each component in the stiffness matrix. However, the model allows for an arbitrary number of terms for  $C_{ij}$  in Eq. 1. It is of interest to find out how many or how few terms are needed in a sufficiently accurate model given the experimental scatter. Looking closely at the plots at  $t = 0$  there is sometimes a considerable difference between model and experimental data. However, the overall trend and behaviour are adequately captured. It is possible to increase the number of Prony terms ( $M$ ) in Eq. (2) to accurately predict the elastic behaviour. However, in the present study, capturing the long term behaviour is the main issue of hand. At this point, the predictive capabilities have however been shown for a straightforward hereditary orthotropic viscoelastic model where the elements in the compliance matrix are described by two terms in the series in Eq. (1). Furthermore, a direct way to handle asymmetric (non-orthotropic) experimental data has been presented in Eqs. (18) and (19). The costs of fixing Poisson's ratios has been investigated, and found to be acceptable only in case it has been experimentally shown that these do not vary with time.

As of right now the model is only able to take into account linear viscoelastic creep and elasticity under constant climate conditions. Therefore, the present model has some limitations: When the model is calibrated against creep data at a given climate condition, the obtained model parameters may only be used at that given climate condition. Thus, if for example the model has been calibrated against creep data of European beech wood at 65% relative humidity and 20 °C, the model will only be valid to be used for structures or components made from European beech wood at 65% relative humidity and 20 °C. The obtained model parameters may be verified by looking for similar experimental data with the same wood species and climate condition, but this has proven to be of great difficulty as there is a lack in creep data in general. Instead, a suggested future work of this study may include a physical experiment of a wooden structure under a constant multi-axial stress state. Then said structure is replicated in a finite element environment using the model calibrated against the same type of wood species and climate condition to assess the generality of the viscoelastic model.

Another common limitation is that the model is only valid during the same duration of the experiment it was calibrated against. If the experimental creep data are 24 h, the model will only be valid for 24 h. To the knowledge of the

authors, predicting creep longer than the given creep data has yet to be explored and requires full understanding of the creep phenomena.

Finally, since the model is intended to be implementable for structural or component simulations in FE codes, limitations regarding scale effects should be addressed. One should then be aware that the assumptions of homogeneity and orthotropy may not be adequate on all length scales for composites and wood materials. The cellular microstructure in wood and the fibrous microstructure of composites affect the mechanical behaviour on the millimetre scale, and the material cannot be regarded as a homogeneous continuum. There is also a risk when using the fitted creep model to simulate larger and complex structures, since the size effects like knots in wood or resin rich pockets in composites etc. are not taken into account. For example the polar orthotropy of wood is not considered here, where Cartesian orthotropic behaviour is assumed.

## Conclusion

Despite the practical importance of creep in wooden and composite structures, experimental data along all main material axes are generally lacking in the literature. In two of the few sources found for wood and fibre composites, one can consider a suitable rheological model that captures the main features, is readily implementable in FE software, but does not overfit the experimental data. For the available experimental data, it can be recommended to use two exponential terms in the Prony series for orthotropic creep. Furthermore, the experimental data generally do not comply with a symmetric creep compliance matrix, as required for orthotropic materials implementation in FE codes. A straightforward scheme to render the creep compliance matrix symmetric is presented in this work.

It has been found to be relatively common in creep to assume that Poisson's ratios are constant and the elastic moduli vary with time. This work shows that fixing the Poisson's ratios is generally not advisable, unless it has been shown that the Poisson's ratios are time-independent in the experimental testing.

Overall, the present scheme provides a fast and direct procedure to formulate a creep model based on experimental data for orthotropic materials like wood and composites. The model can be directly implemented in most FE softwares for creep predictions on a structural or component level.

**Supplementary Information** The online version contains supplementary material available at <https://doi.org/10.1007/s00226-022-01421-x>.

**Funding** Open access funding provided by Uppsala University. This research has been funded by the Swedish Research Council, Grant 2016-04534.

**Code availability** The work has been done in Ansys Mechanical, using an USERMAT subroutine that follows the steps of the implementation described in "Finite element implementation" Section.

**Open Access** This article is licensed under a Creative Commons Attribution 4.0 International License, which permits use, sharing, adaptation, distribution and reproduction in any medium or format, as long as

you give appropriate credit to the original author(s) and the source, provide a link to the Creative Commons licence, and indicate if changes were made. The images or other third party material in this article are included in the article's Creative Commons licence, unless indicated otherwise in a credit line to the material. If material is not included in the article's Creative Commons licence and your intended use is not permitted by statutory regulation or exceeds the permitted use, you will need to obtain permission directly from the copyright holder. To view a copy of this licence, visit <http://creativecommons.org/licenses/by/4.0/>.

## References

- Abouhamzeh M, Sinke J, Jansen KMB et al (2015) A new procedure for thermo-viscoelastic modeling of composites with general orthotropy and geometry. *Compos Struct* 133:871–877. <https://doi.org/10.1016/j.compstruct.2015.08.050>
- Afshar R, Cheylan M, Almkvist G et al (2020) Creep in oak material from the vasa ship: verification of linear viscoelasticity and identification of stress thresholds. *Eur J Wood Prod* 78:1095–1103. <https://doi.org/10.1007/s00107-020-01566-1>
- Alrubraie M, Gardner DJ, Lopez-Anido RA (2020) Modeling the long-term deformation of a geodesic spherical frame structure made from wood plastic composite lumber. *Appl Sci* 10:5017. <https://doi.org/10.3390/app10145017>
- Ando K, Mizutani M, Taniguchi Y et al (2013) Time dependence of Poisson's effect in wood III: asymmetry of three-dimensional viscoelastic compliance matrix of Japanese cypress. *J Wood Sci* 59(4):290–298. <https://doi.org/10.1007/s10086-013-1333-7>
- Bodig J, Jayne BA (1982) *Mechanics of wood and wood composites*
- Eitelberger J, Bader TK, de Borst K et al (2012) Multiscale prediction of viscoelastic properties of softwood under constant climatic conditions. *Comput Mater Sci* 55:303–312. <https://doi.org/10.1016/j.commatsci.2011.11.033>
- Endo VT, de Carvalho Pereira JC (2017) Linear orthotropic viscoelasticity model for fiber reinforced thermoplastic material based on Prony series. *Mech Time Depend Mater* 21:199–221. <https://doi.org/10.1007/s11043-016-9326-8>
- Fortino S, Mirianon F, Toratti T (2009) A 3D moisture-stress FEM analysis for time dependent problems in timber structures. *Mech Time Depend Mater* 13:333–356
- Garab J, Keunecke D, Hering S et al (2010) Measurement of standard and off-axis elastic moduli and Poisson's ratios of spruce and yew wood in the transverse plane. *Wood Sci Technol* 44(3):451–464. <https://doi.org/10.1007/s00226-010-0362-2>
- Gonçalves R, Trinca AJ, Cerri DGP (2011) Comparison of elastic constants of wood determined by ultrasonic wave propagation and static compression testing. In: *Wood and fiber science*, pp 64–75
- Hines WW, Montgomery DC (1980) *Probability and statistics in engineering and management science*. Wiley, Hoboken
- Holzer SM, Loferski JR, Dillard DA (1989) A review of creep in wood: concepts relevant to develop long-term behavior predictions for wood structures. *Wood Fiber Sci* 20:376–392
- Huč S, Svensson S (2018) Influence of grain direction on the time-dependent behaviour of wood analyzed by a 3D rheological model. a mathematical consideration. *Holzforschung* 72:889–897
- Huč S, Svensson S (2018) Coupled two-dimensional modeling of viscoelastic creep of wood. *Wood Sci Technol* 52(1):29–43. <https://doi.org/10.1007/s00226-017-0944-3>
- Melo JD, Radford DW (2003) Viscoelastic characterization of transversely isotropic composite laminate. *J Compos Mater* 37:129–145. <https://doi.org/10.1106/002199803028990>
- Morlier P (1994) *Creep in timber structures*. Taylor and Francis Group, London
- Obara P (2018) Verification of orthotropic model of wood. *Arch Civ Eng*. <https://doi.org/10.2478/ace-2018-0027>
- Ottosen NS, Ristinmaa M (2005) *The mechanics of constitutive modeling*. Elsevier, Amsterdam
- Ozyhar T, Hering S, Niemi P (2013) Viscoelastic characterization of wood: time dependence of the orthotropic compliance in tension and compression. *J Rheol* 57:699–718. <https://doi.org/10.1122/1.4790170>
- Pandini S, Pegoretti A (2008) Time, temperature, and strain effects on viscoelastic Poisson's ratio of epoxy resins. *Polym Eng Sci* 48:1434–1441. <https://doi.org/10.1002/pen.21060>

- Rogers T, Pipkin A (1963) Asymmetric relaxation and compliance matrices in linear viscoelasticity. *Z Angew Math Phys ZAMP* 14:334–343
- Tschoegl NW (2012) *The phenomenological theory of linear viscoelastic behavior: an introduction*. Springer, Berlin
- Tzeng JT (2003) Viscoelastic analysis of composite rotor for pulsed power applications. *IEEE Trans Magn* 39:484–488
- Vidal-Sallé E, Chassagne P (2007) Constitutive equations for orthotropic nonlinear viscoelastic behaviour using a generalized Maxwell model: Application to wood material. *Mech Time Depend Mater* 11:127–142. <https://doi.org/10.1007/s11043-007-9037-2>
- Wen YF, Gibson RF, Sullivan JL (1997) Prediction of momentary transverse creep behavior of thermoplastic polymer matrix composites using micromechanical models. *J Compos Mater* 31(21):2124–2145. <https://doi.org/10.1177/002199839703102101>
- White SR, Kim YK (1998) Process-induced residual stress analysis of AS41350 1–6 composite material. *Mech Compos Mater Struct* 5:153–186
- Zocher MA, Groves SE (1997) A three-dimensional finite element formulation for thermoviscoelastic orthotropic media. *Int J Numer Methods Eng* 40:2267–2288

**Publisher's Note** Springer Nature remains neutral with regard to jurisdictional claims in published maps and institutional affiliations.